Available online at www.sciencedirect.com

SCIENCE DIRECT®

Marine Chemistry 91 (2004) 1–14

MARINE CHEMISTRY

www.elsevier.com/locate/marchem

Sediment accumulation and radionuclide inventories (^{239,240}Pu, ^{210}Pb and ^{234}Th) in the northern Gulf of Mexico, as influenced by organic matter and macrofaunal density

Kevin M. Yeager[a,*], Peter H. Santschi[a], Gilbert T. Rowe[b]

[a] *Laboratory for Oceanographic and Environmental Research, Department of Marine Sciences, Texas A&M University at Galveston, 5007 Ave. U, Galveston, TX 77551, USA*

[b] *Department of Marine Biology, Texas A&M University at Galveston, 5007 Ave. U, Galveston, TX 77551, USA*

Received 28 October 2003; received in revised form 12 March 2004; accepted 17 March 2004
Available online 1 June 2004

Abstract

Six cores were collected from the Northern Gulf of Mexico (GOM) as part of the "Deepwater Program: Northern Gulf of Mexico Continental Slope Habitats and Benthic Ecology" (DGoMB). These cores were collected from water depths ranging from ≈ 700 to 3500 m and processed for radiochemical assays to determine particle reworking (bioturbation) and sedimentation rates in these sediments, pursuant to the research objective to investigate biological, chemical, and physical processes that control the environmental setting for GOM benthic fauna. Bioturbation rates were quantitatively derived from $^{234}Th_{xs}$ profiles, with $^{234}Th_{xs}$ penetration depths ranging between 0.5 and 4 cm, and bioturbation coefficient values (D_b), ranging from ≈ 2 to 30 cm^2/year. $^{234}Th_{xs}$ data were also used to determine the shallow depth limit for particle mixing. Significant values of ^{239,240}Pu were found over the 3–15 cm depth range, without any pronounced peak activities suitable for sediment dating, indicating periodic and nonlocal mixing events. Sedimentation rates (S) were therefore calculated from $^{210}Pb_{xs}$ profiles, assuming steady state conditions, and using the constant flux-constant sedimentation (CF-CS) model. However, only $^{210}Pb_{xs}$ data below the ^{239,240}Pu penetration depth were used for the purpose of determining an upper limit of S. The range of apparent sedimentation rates determined by this approach for these stations is 0.04–0.44 cm/year, after approximately 1000 m depth, sedimentation becomes essentially constant at ≈ 0.08 cm/year. To the best of our knowledge, there are no other published sedimentation rates for the GOM outside the immediate area of the Mississippi River Delta region. However, estimates of sedimentation rates presented here fall in line with rates from similar continental margin marine settings.

^{239,240}Pu and $^{210}Pb_{xs}$ inventories are positively correlated ($r=0.91$, $p=0.01$; $r=0.80$, $p=0.05$, respectively) with macrofauna density, which itself correlates well ($r=0.94$, $p=0.005$) to particulate organic carbon (POC) inventories over the top 5 cm, the approximate average particle mixing (bioturbation) depths of $^{234}Th_{xs}$ at these GOM stations. However, these inventories did not correlate to benthic mixing intensities and depths. High macrofaunal densities and bioturbation intensities are a consequence of elevated rain rates of organic carbon, which is efficiently degraded at the sediment–water interface before incorporation into the sedimentary record. We hypothesize that relatively high densities of macrofauna in a given location on the sea floor, provide for a well mixed near surface sediment layer, wherein fallout radionuclides are more

* Corresponding author. Tel.: +1-409-740-4772; fax: +1-409-740-4786.
E-mail address: yeagerk@tamug.tamu.edu (K.M. Yeager).

0304-4203/$ - see front matter
doi:10.1016/j.marchem.2004.03.016

efficiently incorporated via adsorption and mixing into the sediment profile as compared to locations where macrofaunal densities are less, even when radionuclide fluxes might be similar.

Keywords: Gulf of Mexico; Sedimentation; Bioturbation; Radionuclides; Benthic fauna; Organic carbon

1. Introduction

This research is one component of the "Deepwater Program: Northern Gulf of Mexico Continental Slope Habitats and Benthic Ecology" (DGoMB). This program's focus is on developing an improved understanding of deep-sea areas that will be potentially impacted by current and future exploration and production of fossil fuel reserves in the deep water Gulf of Mexico (GOM), defined as areas with water depths from 300 to 3000 m, located mostly in the Exclusive Economic Zone (EEZ) of the United States. A Gulf-wide perspective is sought to define the structure and function of the deep-sea communities of interest.

Program focus objectives include investigations of: (1) the present condition of biological communities in the study area, (2) distributions and patterns of important deep-sea biota, (3) biological, chemical and physical processes that control the environmental setting, and (4) the effects that these processes have on the character of benthic communities. Radiochemical investigations address point 3 specifically, and it should be noted that work of this type is lacking for the GOM, an understudied basin. In particular, one of the purposes was to assess components of both the

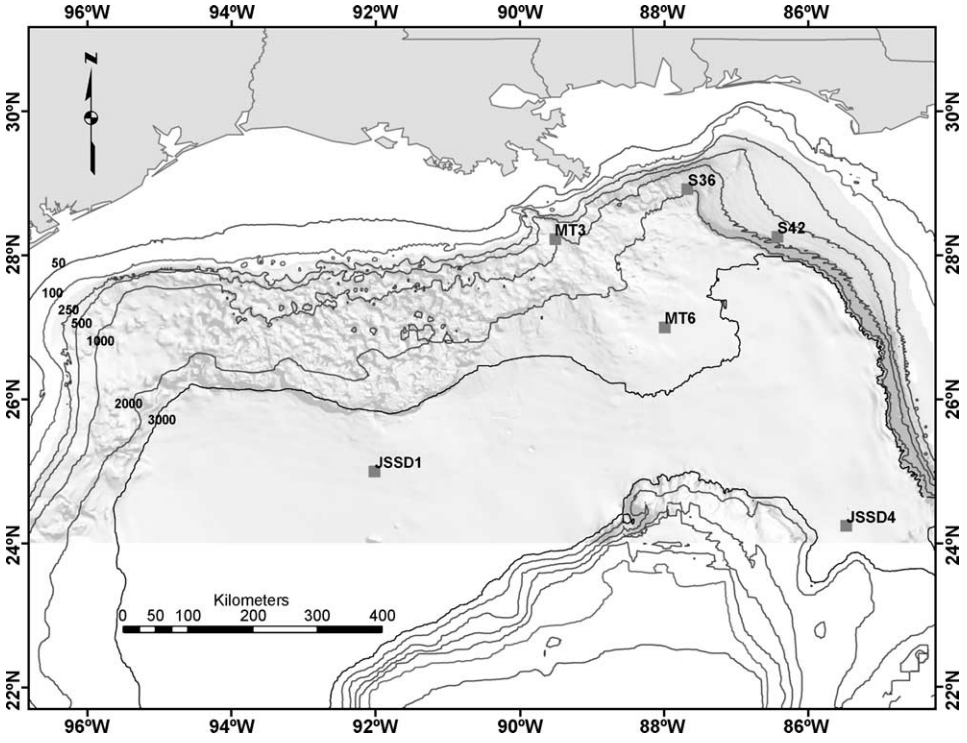

Fig. 1. Bathymetric map of the Northern Gulf of Mexico, showing station locations for cores described herein.

biological (bioturbation depth) and abiotic (sedimentation rate) processes of importance for accomplishing the project objectives, by using a suite of radionuclides including ($^{210}Pb_{xs}$, ^{234}Th and $^{239,240}Pu$). Another purpose was to link these biophysical and sedimentary processes to the incorporation of chemicals such as fallout radionuclides into the sedimentary record by mixing and (re-) adsorption. Ancillary data presented herein include particulate organic carbon (POC) concentrations and macrofaunal densities for each station. A total of six cores, collected on two separate cruises within the northern GOM during the summers of 2001 (Cruise 1) and 2002 (Cruise 3a) are presented here, from stations ranging in water depth from 767 to 3560 m (Fig. 1). Ancillary objectives include: the investigation of relationships between macrofaunal density and both POC and fallout radionuclide inventories and organic carbon remineralization. The importance of this work is manifest, considering that the GOM is understudied in terms of both sediment accumulation and organic carbon data outside of the Mississippi River Delta and plume region.

1.1. Previous research

Fallout radionuclides, including ^{210}Pb (constant fallout) and $^{239,240}Pu$ (episodic fallout since 1945), have been used with success to investigate sedimentation rates in a variety of coastal and marine settings, including deltas (e.g., Goodbred and Kuehl, 1998; Oktay et al., 2000; Santschi et al., 2001a), bays, estuaries and continental shelves (e.g., Santschi et al., 1980; Ravichandran et al., 1995a,b; Huntley et al., 1995; Benoit et al., 1999; Santschi et al., 1999). The radionuclide ^{234}Th has been widely applied to trace particle cycling processes on short times scales near that of its mean life (34 days) and to determine fluxes of POC from the water column (Buesseler et al., 1995; Bacon et al., 1996; Rutgers van der Loeff et al., 1997). One of its main applications has been the determination of bioturbation rates, which can be quantitatively derived from $^{234}Th_{xs}$ profiles (Pope et al., 1996; Santschi et al., 1980, 1999, 2001b).

2. Methods

DGoMB program design included factors believed to be most important in characterizing the biological communities of interest in the GOM, with the idea that an inclusive range of conditions enables an improved understanding of the entire GOM deep-sea benthos, rather than isolated parts. A subset of all survey stations were identified as experimental, or "process" stations, chosen to reflect the greatest range in community dynamics, as inferred from benthic survey data. Cores were collected at a different station in the GOM during the summers of 2001 S42 (Florida Escarpment), S36 (upper Desoto Canyon), MT3 and MT6 (Mississippi Trough) and 2002: JSSD1 and JSSD4 (Sigsbee Deep Abyssal Plain) (Fig. 1; Table 1).

Box cores were collected at each station and subcores for radiochemistry were collected simultaneously; sub-cores (< 30 cm) were frozen on board ship and stored until delivered for analyses. Cores were thawed for 24 h, then sectioned into 0.5 cm intervals over the first 3 cm and sectioned into 1 cm intervals thereafter. Four aliquots of each interval were then divided to allow for: (1) gamma counting (^{234}Th and ^{226}Ra), (2) determination of sedimentary organic carbon (POC) concentrations, (3) determination of $^{239,240}Pu$ concentrations by alpha counting, and (4) determination of ^{210}Pb activity concentrations by alpha counting its granddaughter, ^{210}Po. Bulk samples were dried at 70–80 °C for 24 h, then gently

Table 1
Summary data for all stations, including percent sand, silt and clay for surface sediments at each

Station	Cruise year	Water depth (m)	Latitude	Longitude	%Sand	%Silt	%Clay
S42	2001	767	28°15.16′N	86°25.07′W	20.5	31.4	48.1
MT3	2001	985	28°13.26′N	89°29.71′W	5.9	41.5	52.6
S36	2001	1849	28°55.16′N	87°40.22′W	7.6	41.2	51.1
MT6	2001	2737	27°00′N	87°59.87′W	38.1	21.5	40.4
JSSD1	2002	3520	25°00.42′N	91°59.97′W	21.2	27.7	51.1
JSSD4	2002	3560	24°14.67′N	85°28.27′W	14.9	27.0	58.1

disaggregated with mortar and pestle and passed through 2 and 0.5 mm sieves.

Grain size distributions for sediment surface grab samples at each station were determined by the standard Folk settling method. Fifteen to twenty grams of sediment were treated with hydrogen peroxide for 12 h to remove organic matter. After washing with distilled water, the sediment was dispersed with hexametaphosphate solution and poured over the appropriate screen. The material that passes through the screen was then subjected to a series of prescribed settling techniques that are based on removing materials at set times. Individual fractions collected were dried and weighed to provide quantitative values for each size fraction as a percent of the total weight of sediment. Percent sand, silt, and clay were calculated.

Determination of POC entailed subjecting samples ($\approx$ 1 g) to dilute HCl (2 N) over heat with triplicate rinses to be certain that no inorganic carbon remained. Samples were stored in sealed vials until analyzed. Samples were run in triplicate on a Perkin Elmer Series 2400 Elemental Analyzer (CHNS/O) using standard methods to determine POC (e.g., Santschi et al., 2001b; Yeager and Santschi, 2003).

High-resolution gamma spectrometry was employed to resolve ^{226}Ra ($t_{1/2}$ = 1602 years, via ^{214}Pb Eγ = 352 keV) and ^{234}Th ($t_{1/2}$ = 24.1 days, Eγ = 93 keV) using Canberra HPGe well detectors and a multichannel analyzer, model 747. Samples of $\approx$ 10 g were contained in plastic test tubes (inner diameter 1.3 cm and height 9.4 cm) and sealed with epoxy for 20 days in order for equilibrium between ^{226}Ra and its volatile daughter ^{222}Rn ($t_{1/2}$ = 3.8 days), an inert gas, to be reached. Standards (NIST, SRM #'s 4357 (Ra isotopes) and 4321C (^{234}Th)) were prepared and run on each detector to determine representative efficiencies for each nuclide. Counting and efficiency 1-sigma errors based on standards were less than $\pm$ 2% and all samples were counted, on average, for 3–4 days to reach a standard deviation for ^{226}Ra of $\leq$3–5%. Due to the short half-life of ^{234}Th, it was necessary to gamma count samples immediately. Excess ^{234}Th (^{234}Th$_{xs}$ = total ^{234}Th – (^{234}Th$_{supp}$ = ^{238}U)) was determined by counting a representative subset of samples from each core again, 6 or more months after sample collection, when the only remaining ^{234}Th is that supported directly by decay of its parent, ^{238}U (e.g., Santschi et al., 2001b).

Alpha spectrometry was employed to resolve ^{210}Pb ($t_{1/2}$ = 22.4 years) and ^{239,240}Pu ($t_{1/2} = 24 \times 10^3$ and 6540 years, respectively), using a Canberra alpha spectrometer, model 7404, mated to a Canberra multichannel analyzer, model 8224. Lead-210 samples ($\approx$ 1 g) were spiked with a certified ^{209}Po tracer (Isotope Products Laboratory, #6209-100N) and completely digested (HF, HCl and HNO_3) over heat. Ascorbic acid was then added to bind free Fe(III) and an Ag disk was added to the solution over heat to provide a substrate for spontaneous deposition of polonium isotopes (Santschi et al., 1980, 1999; Ravichandran et al., 1995a,b). Determination of ^{239,240}Pu required wet chemistry to prepare the samples (5–10 g) for analysis, described in detail in Santschi et al. (1980). In summary, this method requires that the sediment samples be leached with 6 M HCl over heat for 24 h and then centrifuged, the tracer ^{242}Pu (NIST, SRM #4334F) was then added and the samples passed through two sets of anion exchange columns (1 × 8, 100–200 mesh) to purify them. Samples were then reconstituted in deionized water (DIW) and plated onto stainless steel planchets by sulfate electrodeposition in preparation for analyses by alpha spectrometry, according to methods described by Santschi et al. (1980, 1999).

Inventories of POC, ^{239,240}Pu and ^{210}Pb$_{xs}$ were determined from porosity determinations and assuming a solid density of 2.5 g/cm^3, according to standard procedures (e.g., Santschi et al., 1999, 2001b). Assuming a value of 2.5 ± 0.1 g/cm^3 for dry density introduces a negligible 1-sigma error into calculated porosities and bulk densities of 1–2%. Errors in calculated inventories were determined by applying the mean percent error of all discrete samples included in the inventory determination to the inventory value. Macrofauna samples were taken with a GOMEX box corer covering an area of 0.2 m^2 (Boland and Rowe, 1991) and a mean penetration depth of 30 cm, followed by sieving through a 300 μm screen to retain the macrofauna. Macrofauna counts were made over the top 15 cm of the core. The samples were then fixed in a 10% buffered formalin and seawater solution. The fauna were then sorted out of the retained sediment into major taxonomic groups in the laboratory, followed by preservation in 70% ethanol.

Table 2
Radionuclide and POC data for station S42, 767 m (mBq/g), errors reported at $\pm 2\sigma$, *= errors < 0.01, and n/d = no data

Depth (cm)	S42							
	Total ^{210}Pb	^{226}Ra	^{210}Pb$_{xs}$	^{234}Th$_{xs}$	^{238}U	^{239,240}Pu	%Porosity	%POC
0.50	421.39 ± 1.61	34.50 ± 1.75	386.89 ± 2.38	165.56 ± 20.37	5.07 ± 1.13	0.45 ± 0.05	0.86	0.80 ± 0.02
1.25	459.88 ± 1.46	33.54 ± 2.03	426.33 ± 2.50	83.67 ± 28.47	6.86 ± 1.24	0.35 ± 0.05	0.81	0.76 ± 0.06
1.75	495.52 ± 0.53	32.58 ± 2.24	462.84 ± 2.30	32.90 ± 28.13	8.05 ± 1.32	0.47 ± 0.10	0.80	0.77 ± 0.00*
2.25	453.99 ± 1.63	31.89 ± 2.20	422.10 ± 2.59	0	n/d	0.21 ± 0.07	0.78	0.72 ± 0.00*
2.75	409.95 ± 0.40	35.23 ± 2.11	374.72 ± 2.14	0	n/d	0.22 ± 0.03	0.78	0.73 ± 0.01
3.25	332.28 ± 0.34	42.18 ± 1.66	290.10 ± 1.70	0	n/d	0.20 ± 0.03	0.73	0.64 ± 0.00*
3.75	259.04 ± 0.77	39.41 ± 1.97	219.63 ± 2.12	0	n/d	0.15 ± 0.02	0.76	0.44 ± 0.00*
4.50	153.38 ± 0.49	39.35 ± 2.27	114.03 ± 2.32	0	n/d	0.20 ± 0.03	0.77	n/d
5.50	142.87 ± 0.46	40.64 ± 2.25	102.23 ± 2.29	0	n/d	0.10 ± 0.01	0.75	n/d
6.50	39.56 ± 0.23	34.10 ± 1.09	5.45 ± 1.11	0	n/d	0.06 ± 0.00*	0.74	n/d
7.50	65.49 ± 0.21	29.94 ± 2.10	35.55 ± 2.11	0	n/d	0.04 ± 0.02	0.75	n/d
8.50	44.80 ± 0.18	29.31 ± 0.99	15.49 ± 1.00	0	n/d	0	0.73	0.46 ± 0.00*
9.50	43.67 ± 0.14	29.06 ± 1.18	14.61 ± 1.18	0	n/d	n/d	0.72	n/d
10.50	42.93 ± 0.13	26.31 ± 1.63	16.62 ± 1.64	0	n/d	n/d	0.72	n/d
11.50	41.96 ± 0.15	27.78 ± 0.92	14.18 ± 0.94	0	n/d	0.42 ± 0.09	0.71	n/d
12.50	37.44 ± 0.14	30.96 ± 1.03	6.48 ± 1.04	0	n/d	0	0.70	n/d
13.50	35.26 ± 0.17	29.67 ± 0.93	5.60 ± 0.94	0	n/d	n/d	0.73	0.46 ± 0.00*
14.50	36.97 ± 0.50	28.97 ± 1.34	8.00 ± 1.43	0	n/d	0.09 ± 0.01	0.69	n/d
15.50	33.52 ± 0.13	27.17 ± 0.87	6.35 ± 0.88	0	n/d	n/d	0.74	n/d
17.50	31.70 ± 0.10	27.34 ± 0.86	4.36 ± 0.87	0	n/d	n/d	0.74	n/d
18.50	n/d	n/d	n/d	0	n/d	n/d	0.73	0.46 ± 0.00*

Table 3
Radionuclide and POC data for station MT3, 985 m (mBq/g), errors reported at $\pm 2\sigma$, *= errors < 0.01, n/d = no data, and italics=[^{238}U] based on best fit to actual measurements

Depth (cm)	MT3							
	Total ^{210}Pb	^{226}Ra	^{210}Pb$_{xs}$	^{234}Th$_{xs}$	^{238}U	^{239,240}Pu	%Porosity	%POC
0.50	845.59 ± 3.41	42.47 ± 2.15	803.12 ± 4.03	108.74 ± 19.11	14.57 ± 1.73	0.44 ± 0.05	0.91	1.31 ± 0.01
1.25	842.62 ± 2.78	48.48 ± 2.33	794.14 ± 3.63	134.93 ± 23.52	*17.07 ± 1.70*	0.52 ± 0.05	0.84	1.62 ± 0.01
1.75	815.04 ± 4.19	52.47 ± 2.51	762.57 ± 4.88	105.49 ± 26.49	*18.73 ± 1.87*	8.10 ± 0.94	0.84	1.49 ± 0.01
2.25	897.38 ± 3.22	52.94 ± 1.81	844.44 ± 3.70	86.99 ± 20.55	20.40 ± 1.88	0.47 ± 0.06	0.85	1.49 ± 0.01
2.75	846.76 ± 3.06	42.56 ± 2.20	804.20 ± 3.77	39.62 ± 26.02	*22.07 ± 2.20*	1.24 ± 0.13	0.86	1.65 ± 0.01
3.25	891.52 ± 3.52	48.80 ± 2.01	842.72 ± 4.06	22.93 ± 19.02	*23.73 ± 2.37*	1.07 ± 0.11	0.85	1.44 ± 0.01
3.75	802.68 ± 2.28	36.54 ± 1.65	766.14 ± 2.82	0	25.40 ± 3.08	3.48 ± 0.47	0.82	1.43 ± 0.01
4.50	786.24 ± 3.10	46.55 ± 1.67	739.70 ± 3.52	0	n/d	0.48 ± 0.05	0.84	n/d
5.50	785.69 ± 2.35	37.86 ± 1.35	746.93 ± 2.71	0	n/d	0.55 ± 0.06	0.84	n/d
6.50	472.47 ± 2.05	38.43 ± 1.17	434.04 ± 2.36	0	n/d	0.49 ± 0.05	0.84	n/d
7.50	469.08 ± 1.11	45.38 ± 1.64	423.70 ± 1.98	0	n/d	0.49 ± 0.05	0.84	n/d
8.50	568.52 ± 2.20	39.48 ± 1.18	529.05 ± 2.50	0	n/d	1.07 ± 0.22	0.85	0.95 ± 0.00*
9.50	493.48 ± 1.57	39.31 ± 1.33	454.17 ± 2.06	0	n/d	0.31 ± 0.05	0.84	n/d
10.50	567.36 ± 1.22	49.89 ± 2.01	517.47 ± 2.35	0	n/d	2.22 ± 0.22	0.82	n/d
11.50	515.00 ± 1.53	44.13 ± 1.40	470.84 ± 2.08	0	n/d	1.82 ± 0.18	0.81	n/d
12.50	467.75 ± 1.62	38.70 ± 1.32	429.05 ± 2.09	0	n/d	0.35 ± 0.04	0.80	n/d
13.50	498.26 ± 1.23	34.03 ± 1.75	464.23 ± 2.14	0	n/d	0.30 ± 0.03	0.75	0.97 ± 0.00*
14.50	15.64 ± 0.12	27.57 ± 1.07	0	0	n/d	0.04 ± 0.25	0.73	n/d
15.50	139.18 ± 0.42	30.49 ± 1.13	108.69 ± 1.21	0	n/d	n/d	0.77	n/d
16.50	48.91 ± 0.25	30.96 ± 1.73	17.95 ± 1.75	0	n/d	0.02 ± 0.00*	0.77	n/d
17.50	48.10 ± 0.17	28.06 ± 1.06	20.03 ± 1.08	0	n/d	n/d	0.77	n/d
18.50	n/d	n/d	n/d	0	n/d	0.09 ± 0.01	n/d	0.95 ± 0.00*
19.50	42.99 ± 0.12	30.27 ± 1.72	12.72 ± 1.72	0	n/d	n/d	0.72	n/d

3. Results and discussion

Primary data for all stations, including total ^{210}Pb, ^{226}Ra, ^{210}Pb$_{xs}$, ^{234}Th$_{xs}$, ^{238}U, ^{239,240}Pu, %POC and porosity are shown in Tables 2–7. ^{234}Th$_{xs}$ data from station S36 are not available, due to the large number of samples, as samples were counted too long after collection ($t_{1/2}$ = 24 days). These data are used to calculate particle reworking (bioturbation), sedimentation and accumulation rates in these sediments, as discussed in detail below. The fallout radionuclides ^{137}Cs and ^{7}Be were not resolved at sufficient activities in any core to be useful.

3.1. Bioturbation rates

The fauna found at these stations are typical for fine-grained, deep ocean sediments. Polychaetes and nematodes were numerically dominant, followed by crustaceans (isopods, amphipods and cumaceans), and bivalve molluscs. Most of the fauna were deposit feeders, which is again typical of the deep ocean.

Bioturbation rates can be quantitatively derived from ^{234}Th$_{xs}$ profiles as described by Santschi et al. (1980, 1999) and from the analysis of peak shapes of different tracer concentration profiles. ^{234}Th$_{xs}$ profiles, which are calculated as the difference between ^{234}Th (total) and supported ^{234}Th (^{234}Th$_{supp}$ = ^{238}U), were used to determine particle reworking (bioturbation) rate coefficients, D_b, shown in Fig. 2 and listed in Table 8 along with mixing depths, inventories, macrofaunal densities and other station data. Assuming steady state conditions, D_b is calculated as follows:

$$[^{234}\mathrm{Th}_{xs}(z)] = [^{234}\mathrm{Th}_{xs}(0)]\exp(-(\lambda/D_b)^{1/2}z) \quad (1)$$

where λ = decay constant of ^{234}Th (0.0288 day^{-1}), and z = depth. Numerical mixing and sedimentation models discussed in Santschi et al. (2001b) illustrate that the

Table 4
Radionuclide and POC data for station S36, 1849 m (mBq/g), *= errors < 0.01, n/d = no data, and italics=[^{238}U] based on best fit to actual measurements

Depth (cm)	S36							
	Total ^{210}Pb	^{226}Ra	^{210}Pb$_{xs}$	^{234}Th$_{xs}$	^{238}U	^{239,240}Pu	%Porosity	%POC
0.50	542.43 ± 3.31	33.37 ± 1.98	509.06 ± 3.86	n/d	15.69 ± 1.85	1.59 ± 0.25	0.89	0.84 ± 0.05
1.25	419.78 ± 2.01	32.99 ± 1.04	386.78 ± 2.26	n/d	n/d	0.88 ± 0.09	0.85	1.03 ± 0.00*
1.75	421.75 ± 1.54	35.35 ± 0.98	386.40 ± 1.83	n/d	n/d	0.16 ± 0.03	0.80	0.98 ± 0.00*
2.25	542.16 ± 2.85	42.02 ± 1.18	500.14 ± 3.08	n/d	n/d	0.36 ± 0.05	0.81	0.92 ± 0.05
2.75	735.92 ± 4.02	37.69 ± 2.15	698.23 ± 4.56	n/d	n/d	1.66 ± 0.17	0.82	1.17 ± 0.01
3.25	668.48 ± 2.96	35.22 ± 1.03	633.26 ± 5.23	n/d	n/d	0.02 ± 0.00*	0.79	0.91 ± 0.07
3.75	602.62 ± 2.43	32.78 ± 1.09	569.84 ± 2.66	n/d	n/d	0.57 ± 0.06	0.78	0.94 ± 0.00*
4.50	473.52 ± 1.10	33.64 ± 0.99	439.88 ± 1.48	n/d	*16.10 ± 1.61*	0.42 ± 0.04	0.83	n/d
5.50	470.41 ± 1.81	38.66 ± 1.56	431.75 ± 2.39	n/d	n/d	1.12 ± 0.10	0.81	n/d
6.50	199.93 ± 0.72	33.79 ± 0.97	166.14 ± 1.21	n/d	n/d	0.19 ± 0.02	0.80	n/d
7.50	189.68 ± 0.76	40.12 ± 1.28	149.56 ± 1.49	n/d	*16.49 ± 1.65*	0.06 ± 0.01	0.80	n/d
8.50	105.49 ± 0.34	40.59 ± 1.15	64.91 ± 1.20	n/d	n/d	0.01 ± 0.01	0.80	0.67 ± 0.00*
9.50	108.42 ± 0.38	42.96 ± 1.91	65.46 ± 1.94	n/d	17.34 ± 1.88	0	0.80	n/d
10.50	117.14 ± 0.42	44.46 ± 1.46	72.68 ± 1.52	n/d	n/d	0.07 ± 0.01	0.80	n/d
11.50	113.70 ± 0.39	44.13 ± 1.40	69.60 ± 1.46	n/d	*17.00 ± 1.70*	0.11 ± 0.01	0.79	n/d
12.50	114.32 ± 0.42	78.45 ± 2.04	35.87 ± 2.09	n/d	n/d	1.20 ± 0.14	0.78	n/d
13.50	106.94 ± 0.35	100.34 ± 3.30	6.59 ± 3.32	n/d	n/d	n/d	0.78	0.83 ± 0.00*
14.50	169.56 ± 0.57	120.31 ± 2.98	49.26 ± 3.04	n/d	*17.39 ± 1.74*	1.09 ± 0.10	0.78	n/d
15.50	152.69 ± 0.52	30.49 ± 1.13	122.21 ± 1.25	n/d	n/d	2.15 ± 0.24	0.78	n/d
16.50	118.52 ± 0.43	76.32 ± 1.96	42.19 ± 2.00	n/d	*17.65 ± 1.77*	0.01 ± 0.00*	0.76	n/d
17.50	121.14 ± 0.43	40.73 ± 1.79	80.42 ± 1.84	n/d	17.07 ± 2.47	0.26 ± 0.03	0.77	n/d
18.50	55.44 ± 0.19	38.23 ± 1.12	17.21 ± 1.14	n/d	n/d	n/d	0.78	0.74 ± 0.00*
19.50	50.52 ± 0.18	38.39 ± 1.11	12.14 ± 1.13	n/d	n/d	0	0.73	n/d
20.50	41.95 ± 0.13	37.85 ± 1.21	4.10 ± 1.22	n/d	n/d	0	0.75	n/d
22.50	49.98 ± 0.13	38.48 ± 1.52	11.50 ± 1.52	n/d	n/d	n/d	0.45	n/d

Table 5
Radionuclide and POC data for station MT6, 2737 m (mBq/g), errors reported at $\pm 2\sigma$, *= errors < 0.01, n/d = no data, and italics=[^{238}U] based on best fit to actual measurements

Depth (cm)	MT6							
	Total ^{210}Pb	^{226}Ra	^{210}Pb$_{xs}$	^{234}Th$_{xs}$	^{238}U	^{239,240}Pu	%Porosity	%POC
0.50	369.08 ± 1.18	22.27 ± 1.05	346.81 ± 1.58	157.22 ± 18.9	16.77 ± 2.10	0.47 ± 0.07	0.87	0.45 ± 0.00*
1.25	89.50 ± 0.33	25.98 ± 1.15	63.51 ± 1.20	27.01 ± 19.77	*17.56 ± 2.20*	0.07 ± 0.05	0.81	n/d
1.75	54.58 ± 0.20	26.68 ± 0.94	27.90 ± 0.96	522.49 ± 106.95	*18.08 ± 2.26*	0.29 ± 0.04	0.81	n/d
2.25	54.92 ± 0.24	25.72 ± 1.16	29.20 ± 1.19	98.78 ± 81.83	*18.61 ± 2.30*	n/d	0.78	0.56 ± 0.04
2.75	56.24 ± 0.23	25.79 ± 0.79	30.44 ± 0.82	8.00 ± 17.33	19.14 ± 2.40	0.04 ± 0.01	0.74	0.39 ± 0.02
3.25	61.69 ± 0.24	25.78 ± 0.90	35.92 ± 0.93	49.81 ± 75.16	*19.66 ± 2.46*	0.10 ± 0.02	0.79	0.68 ± 0.00*
3.75	60.55 ± 0.25	25.16 ± 0.76	35.39 ± 0.80	0	n/d	n/d	0.74	0.38 ± 0.00*
4.50	61.33 ± 0.25	26.94 ± 0.78	34.39 ± 0.82	0	n/d	0.05 ± 0.01	0.77	n/d
5.50	66.66 ± 0.24	26.98 ± 0.91	39.68 ± 0.94	0	22.03 ± 2.75	n/d	0.77	n/d
6.50	72.83 ± 0.22	31.55 ± 0.89	41.29 ± 0.91	0	n/d	n/d	0.77	n/d
7.50	76.89 ± 0.31	40.45 ± 1.13	36.43 ± 1.17	0	n/d	0.08 ± 0.01	0.79	n/d
8.50	64.91 ± 0.24	30.91 ± 1.37	33.99 ± 1.39	0	n/d	n/d	0.79	0.41 ± 0.00*
9.50	52.82 ± 0.22	32.02 ± 1.06	20.80 ± 1.08	0	n/d	n/d	0.75	n/d
10.50	64.49 ± 0.22	32.59 ± 1.12	31.90 ± 1.14	0	n/d	0.03 ± 0.00*	0.73	n/d
11.50	62.60 ± 0.23	31.19 ± 1.06	31.45 ± 1.08	0	n/d	0.06 ± 0.01	0.79	n/d
12.50	n/d	n/d	n/d	n/d	n/d	0	n/d	n/d
13.50	44.65 ± 0.19	25.61 ± 0.86	19.04 ± 0.88	0	n/d	1.11 ± 0.10	0.77	1.37 ± 0.01
14.50	n/d	n/d	n/d	n/d	n/d	0.02 ± 0.00*	n/d	n/d
15.50	32.55 ± 0.13	24.81 ± 0.89	7.75 ± 0.90	0	n/d	0.12 ± 0.06	0.77	n/d
16.50	n/d	n/d	n/d	n/d	n/d	0	n/d	n/d
17.50	33.07 ± 0.14	27.49 ± 0.87	5.58 ± 0.88	0	n/d	n/d	0.74	n/d
18.50	n/d	n/d	n/d	n/d	n/d	0	0.72	0.60 ± 0.00*
19.50	n/d	n/d	n/d	n/d	n/d	n/d	0.75	n/d
20.50	n/d	n/d	n/d	n/d	n/d	0.80 ± 0.08	0.75	n/d
22.50	n/d	n/d	n/d	n/d	n/d	n/d	n/d	n/d

constant D_b model is conservative in that it tends to under predict mixing rates in the near-surface layer.

^{234}Th$_{xs}$ penetration depths are between 0.5 and 4 cm, and bioturbation coefficient values, D_b, range from approximately 2 to 30 cm^2/year. Because particle reworking or bioturbation rates are expected to decrease exponentially with depth, coincident with the depth distribution of benthic infauna (Stull et al., 1996), it is not likely that the depth of more intensively mixed sediment is much higher than that observed by ^{234}Th$_{xs}$. The longer "memory" of the fallout radionuclides ^{210}Pb$_{xs}$ and ^{239,240}Pu do indicate deeper penetration depths than ^{234}Th$_{xs}$ as summarized in Table 8 for all but the deepest stations. This is not surprising, while active mixing is certainly confined to the upper few centimeters, as reflected by ^{234}Th$_{xs}$ data, the relatively long lived radionuclides ^{210}Pb$_{xs}$ and ^{239,240}Pu ($t_{1/2}$ = 22, 24×10^3 and 6540 years, respectively) combined with low sedimentation and accumulation rates and nonlocal episodic mixing events, results in penetration depths for these isotopes which are often considerably deeper. In deep water, such as for stations JSSD1 and JSSD4 (3520, 3560 m, respectively), there is very little ^{239,240}Pu and the penetration depths for ^{234}Th$_{xs}$ and ^{210}Pb$_{xs}$ are essentially the same.

3.2. Sedimentation and accumulation rates

According to the constant flux-constant sedimentation (CF-CS) model, sedimentation rates can be calculated assuming steady state conditions and at relatively constant porosity, using:

$$[^{210}\mathrm{Pb}_{xs}(z)] = [^{210}\mathrm{Pb}_{xs}(0)]\exp(-\alpha z) \quad (2a)$$

$$\alpha = (\lambda/S) \quad (2b)$$

Table 6
Radionuclide and POC data for station JSSD1, 3520 m (mBq/g), errors reported at ± 2σ, *= errors < 0.01, n/d = no data, and italics=[^{226}Ra] based on best fit to actual measurements

Depth (cm)	JSSD1							
	Total ^{210}Pb	^{226}Ra	^{210}Pb$_{xs}$	^{234}Th$_{xs}$	^{238}U	^{239,240}Pu	%Porosity	%POC
0.50	506.70 ± 22.95	19.67 ± 1.17	487.03 ± 22.99	136.63 ± 23.09	n/d	0	0.77	0.56 ± 0.00*
1.25	183.44 ± 4.92	73.47 ± 6.85	109.97 ± 8.43	10.56 ± 22.84	n/d	0.06 ± 0.03	0.73	0.13 ± 0.00*
1.75	234.30 ± 6.14	73.07 ± 7.16	161.23 ± 9.43	13.50 ± 26.30	n/d	0	0.70	0.50 ± 0.00*
2.25	155.84 ± 5.57	67.17 ± 6.48	88.67 ± 8.55	0	n/d	0	0.69	0.50 ± 0.00*
2.75	114.93 ± 3.53	65.18 ± 6.27	49.75 ± 7.20	0	n/d	0.03 ± 0.00*	0.72	0.48 ± 0.00*
3.25	93.72 ± 4.11	*67.62 ± 8.22*	26.10 ± 9.19	0	n/d	0	0.72	0.60 ± 0.05
3.75	64.37 ± 2.44	*70.03 ± 8.36*	0	n/d	n/d	0	0.71	0.44 ± 0.03
4.25	93.74 ± 3.34	*72.46 ± 8.51*	21.28 ± 9.14	n/d	n/d	0	0.72	0.76 ± 0.04
4.75	95.01 ± 4.05	74.88 ± 7.88	20.13 ± 8.86	n/d	n/d	0.04 ± 0.03	0.68	0.44 ± 0.02
5.50	81.70 ± 3.71	*79.17 ± 8.89*	2.53 ± 9.63	n/d	n/d	n/d	0.73	0.48 ± 0.00*
6.50	53.26 ± 3.25	n/d	n/d	n/d	n/d	n/d	0.75	0.33 ± 0.00*
7.50	43.55 ± 2.42	n/d	n/d	n/d	n/d	n/d	0.75	0.48 ± 0.00*
8.50	45.30 ± 2.07	96.28 ± 9.88	0	n/d	18.95 ± 6.14	n/d	0.74	0.42 ± 0.02
9.50	54.70 ± 2.45	n/d	n/d	n/d	n/d	n/d	0.67	0.30 ± 0.00*
10.50	39.15 ± 2.48	n/d	n/d	n/d	n/d	n/d	0.76	0.12 ± 0.00*
11.50	43.16 ± 2.19	n/d	n/d	n/d	n/d	n/d	0.65	0.33 ± 0.00*
12.50	42.34 ± 3.24	101.84 ± 9.35	0	n/d	n/d	n/d	0.64	0.38 ± 0.02
13.50	54.50 ± 3.49	n/d	n/d	n/d	n/d	n/d	0.70	0.13 ± 0.00*
14.50	70.30 ± 4.05	n/d	n/d	n/d	n/d	n/d	0.67	0.33 ± 0.02
15.50	83.12 ± 4.12	n/d	n/d	n/d	n/d	n/d	0.78	0.32 ± 0.02
16.50	73.80 ± 3.31	148.16 ± 13.32	0	n/d	20.19 ± 4.66	n/d	0.65	n/d
18.00	46.84 ± 2.80	n/d	n/d	n/d	n/d	n/d	0.60	n/d

where [^{210}Pb$_{xs}(z)$] and [^{210}Pb$_{xs}(0)$] represent excess ^{210}Pb concentration at depth z and at the sediment interface, respectively; S = sedimentation rate (cm/year); λ = decay constant of ^{210}Pb (0.031 year^{-1}). As sediment porosity was nearly constant over the depth intervals modeled for S, sediment accumulation rates were also determined using:

$$\mathrm{SA} = S[(1-\phi)(\rho)] \quad (3)$$

where SA = sediment accumulation rate (g/cm^2 year), ϕ = porosity, i.e., sediment percent pore space and ρ = sediment bulk density (2.5 g/cm^3).

The CF-CS method also assumes that particle reworking rates are not significant over the depth interval of the ^{210}Pb profile, and that fluxes of both sediments and ^{210}Pb have been constant. ^{234}Th$_{xs}$ data were also used to determine the shallow depth limit for particle mixing, all ^{210}Pb$_{xs}$ data below this depth were then plotted in semi-log format (Fig. 3), then only those ^{210}Pb$_{xs}$ data below the deep limit mixing depth, as defined by the depth where significant ^{239,240}Pu activities cease, were used to determine an upper limit for both sedimentation rates (S) and sediment accumulation rates (SA). While ^{239,240}Pu data were not of sufficient resolution to accurately mark discrete temporal stratifications within the sediment profiles based on known high fallout years, they were sufficient to illustrate depth intervals within the sediment profiles where local or nonlocal mixing was suspected (worm burrows, etc.). Inventories, mixing depths and modeled parameters are summarized for each station in Table 8.

The ranges of apparent sedimentation and accumulation rates determined by this approach for these stations are 0.04–0.44 cm/year and 0.02–0.56 g/cm^2/year, respectively, showing that after approximately 1000 m water depth, sedimentation and accumulation rates become essentially constant at approximately 0.08 cm/year, and 0.04 g/cm^2 year, respectively, within the error. Apparent sedimentation and accumulation rates could not be corroborated here through use of a second tracer

Table 7
Radionuclide and POC data for station JSSD4, 3560 m (mBq/g), errors reported at $\pm 2\sigma$, *= errors <0.01, n/d = no data, and italics=[^{226}Ra] based on best fit to actual measurements

Depth (cm)	JSSD4							
	Total ^{210}Pb	^{226}Ra	^{210}Pb$_{xs}$	^{234}Th$_{xs}$	^{238}U	^{239,240}Pu	%Porosity	%POC
0.50	288.63 ± 8.75	45.55 ± 5.20	243.08 ± 10.18	32.92 ± 36.98	n/d	0	0.83	0.22 ± 0.01
1.25	238.22 ± 10.05	53.76 ± 5.40	184.46 ± 11.41	0	8.01 ± 4.55	0	0.69	0.26 ± 0.00*
1.75	157.13 ± 6.18	50.42 ± 5.71	106.71 ± 8.41	0	n/d	0	0.69	0.31 ± 0.00*
2.25	105.76 ± 3.76	68.15 ± 6.90	37.61 ± 7.86	0	n/d	0	0.63	0.16 ± 0.00*
2.75	89.56 ± 3.86	68.03 ± 7.28	21.53 ± 8.24	0	n/d	0.04 ± 0.00*	0.63	n/d
3.25	84.11 ± 3.96	*63.75 ± 7.98*	20.36 ± 8.91	n/d	n/d	0.02 ± 0.01	0.67	0.36 ± 0.02
3.75	79.22 ± 3.04	*59.47 ± 7.71*	19.75 ± 8.29	n/d	n/d	0	0.61	0.36 ± 0.00*
4.25	74.51 ± 2.85	*55.19 ± 7.42*	19.32 ± 7.95	n/d	10.37 ± 5.63	n/d	0.64	0.39 ± 0.03
4.75	72.92 ± 3.58	50.91 ± 7.61	22.01 ± 8.41	n/d	n/d	n/d	0.67	0.27 ± 0.00*
5.50	70.73 ± 3.53	*55.26 ± 7.43*	15.47 ± 8.23	n/d	n/d	n/d	0.79	0.29 ± 0.00*
6.50	55.86 ± 2.10	*61.08 ± 7.82*	0	n/d	n/d	n/d	0.74	0.48 ± 0.00*
7.50	53.53 ± 2.01	n/d	n/d	n/d	n/d	n/d	0.76	0.41 ± 0.00*
8.50	54.78 ± 2.20	72.74 ± 7.39	0	n/d	n/d	n/d	0.78	0.31 ± 0.02
9.50	36.55 ± 1.51	n/d	n/d	0	n/d	n/d	0.73	0.29 ± 0.00*
10.50	44.82 ± 1.93	n/d	n/d	n/d	n/d	0	0.69	0.28 ± 0.02
11.50	45.54 ± 1.77	n/d	n/d	n/d	17.73 ± 4.01	0	0.72	0.36 ± 0.00*
12.50	44.97 ± 1.98	83.50 ± 7.67	0	n/d	n/d	n/d	0.73	n/d
13.50	n/d	n/d	n/d	0	n/d	n/d	n/d	0.25 ± 0.00*
14.00	45.54 ± 2.26	90.52 ± 7.89	0	n/d	n/d	n/d	0.61	n/d
14.50	n/d	n/d	n/d	n/d	n/d	n/d	n/d	0.25 ± 0.00*
15.50	n/d	n/d	n/d	n/d	18.84 ± 4.21	0	n/d	0.24 ± 0.00*
17.50	n/d	n/d	n/d	n/d	n/d	n/d	n/d	n/d
18.50	n/d	n/d	n/d	n/d	n/d	n/d	n/d	n/d
19.50	n/d	n/d	n/d	n/d	n/d	n/d	n/d	n/d
20.50	n/d	n/d	n/d	n/d	n/d	n/d	n/d	0.20 ± 0.00*

radionuclide (^{137}Cs or ^{239,240}Pu). The 1963 peak for either ^{137}Cs or ^{239,240}Pu would likely have been obliterated, as these apparent sedimentation and accumulation rates combined with the mixing depths evident at these stations would have placed those peaks in the strongly bioturbated top few centimeters. No other data exists on sedimentation or accumulation rates at these GOM stations, either as part of this research effort or in the literature, in fact, reliable, published sedimentation rates for the GOM outside the immediate area of the Mississippi River Delta region are essentially nonexistent in the literature. The estimates of sedimentation rates and sediment accumulation rates presented here do fall in line with rates from similar continental margin marine settings, including the northwestern Mediterranean Sea (0.01–0.60 cm/year, Zuo et al., 1997), the eastern Arabian Sea (0.06–0.66 cm/year, Somayajulu et al., 1999), the Bay of Biscay, northeastern Atlantic (0.06–0.4 cm/year, Radakovitch and Heussner, 1999) and the middle Atlantic Bight (0.03–0.04 cm/year, 0.02–0.05 g/cm^2 year Anderson et al., 1994; 0.003–0.12 cm/year, DeMaster et al., 2002).

3.3. Importance of macrofauna and organic carbon

Macrofaunal densities were determined for each station and are shown in Table 8. The abundance of macrofauna, particularly on the floor of the deep ocean, is dominantly controlled by the abundance and availability of organic carbon. Roughly linear relationships have been shown between macrofaunal abundance and organic carbon rain rates in varied marine environments (western North Atlantic, Rowe et al., 1991; northeast Atlantic, Legeleux et al., 1994; and the North Carolina continental margin, DeMaster et al., 1994). The average particle mixing (bioturbation) depths at these GOM stations is less than 5 cm, and the majority of macrofauna counted were found concentrated in the near surface (0–5 cm depth). POC inventories were

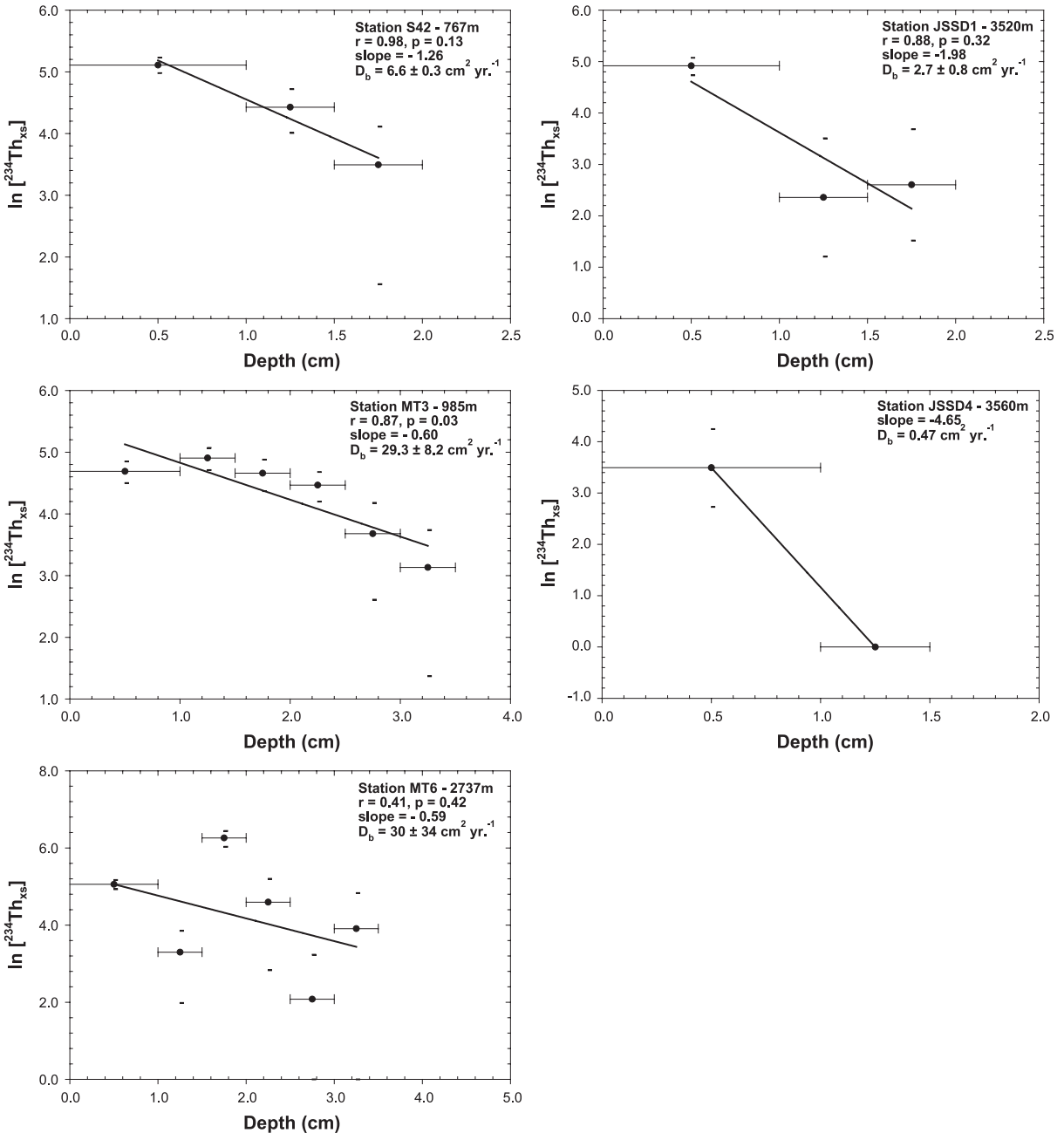

Fig. 2. $^{234}Th_{xs}$ ($[^{234}Th(total)] - [^{238}U]$) penetration into surface sediments at each station, allowing determination of particle reworking (bioturbation) rate (D_b) and depth (z_m), units are mBq/g. D_b was calculated from the slope of $\ln[^{234}Th_{xs}(z)] = \ln[^{234}Th_{xs}(0)] - (\lambda/D_b)^{1/2}z$. Errors in ln $^{234}Th_{xs}$ data are plotted for each point, but are sometimes less than the size of the data symbol.

Table 8
Summary data and modeling results for all stations, errors reported at $\pm 2\sigma$, n/d or nd = no data, D_b values determined using $^{234}Th_{xs}$ data

Station	Depth (m)	$^{210}Pb_{xs}$ inventory (Bq/cm^2)	$^{239,240}Pu$ inventory (mBq/cm^2)	POC inventory (upper 5 cm) (mg/cm^2)	Bioturbation coefficient (D_b) (cm^2/year)	Bioturbation depth (cm) $^{234}Th_{xs}/^{210}Pb_{xs}$	Macrofaunal density (n/m^2)	Sedimentation rate (cm/year)	Accumulation rate (g/cm^2 year)
S42	767	0.96 ± 0.07	1.66 ± 0.33	14.3 ± 0.5	6.6 ± 0.3	1.75/2	4520	0.44 (0.26–1.55)[a]	0.36–0.76[a]
MT3	985	3.48 ± 0.07	6.83 ± 0.82	21.5 ± 0.2	29.3 ± 8.2	3.25/15	13,299	0.07 ± 0.06	0.03 ± 0.02
S36	1849	1.81 ± 0.12	5.53 ± 1.1	20.2 ± 0.6	n/d	nd/15.50	16,243	0.09 ± 0.05	0.05 ± 0.03
MT6	2737	0.35 ± 0.01	1.89 ± 0.45	11.8 ± 0.2	30 ± 34	3.25/12.50	1919	0.10 ± 0.03	0.05 ± 0.01
JSSD1	3520	0.97 ± 0.28	0.07 ± 0.02	14.5 ± 1.2	2.7 ± 0.8	1.75/2	3745	0.04 ± 0.01	0.02 ± 0.01
JSSD4	3560	0.69 ± 0.21	0.02 ± 0.01	11.2 ± 0.5	0.47[b]	1.75/2	1893	0.08 ± 0.03	0.04 ± 0.02

[a] An upper and lower limit for S are listed for this station due to a high error, resulting from few points available below the $^{239,240}Pu$ penetration depth at this station.
[b] D_b determined based on one data point, extrapolated to zero at depth (Fig. 2).

determined to this depth (Table 8) and compared directly with macrofaunal densities, illustrating that these data significantly support this relationship in place also in the GOM (Fig. 4).

The density of macrofauna also significantly influences inventories of fallout radionuclides, including $^{239,240}Pu$ and $^{210}Pb_{xs}$ (Fig. 5A,B). Organic carbon raining on sediments fuels secondary production, benthic respiration and macrofaunal biomass. Organic carbon that survives degradation processes at or near the sediment water interface also fuels diagenetic processes within the sediments. Benthic macrofaunal biomass is thus a consequence of multiple factors, foremost being food supply through organic carbon rain from the euphotic zone of the ocean. We hypothesize that relatively high densities of macrofauna in a given location on the sea floor, provide for a well mixed near surface sediment layer. In this setting, fallout radionuclides are more efficiently incorporated via mixing and adsorption into the sediment profile as compared to locations where macrofaunal densities are less, even when radionuclide fallout rates are similar, resulting in the observed significant relationship between the two variables.

The determination of organic carbon remineralization at these stations was also investigated, according to methods described in detail in Anderson et al. (1994). Only one station, S42, was suitable for this analysis. Over the mixed layer at this station, as defined by $^{234}Th_{xs}$ (1.75 cm), the POC gradient was determined (-1.43 ± 0.55 mg/cm^4) as was the organic carbon remineralization rate (259 ± 101 mg/m^2 day). While this remineralization value is of the same order of magnitude as data reported for similarly shallow sediments in the mid-Atlantic Bight by Anderson et al. (1994), comparison with organic carbon influx and efflux determinations (sediment accumulation rate × POC concentration) through this depth range (0–1.75 cm) show that mass balance is not attained. This discrepancy may be due to: (a) the very small depth range over which the determination was made, (b) the limitations inherent in the application of a steady state model to measure a non-steady state process, or most likely, (c) a combination of a and b.

4. Summary and conclusions

Six cores were collected from the northern GOM as part of the "Deepwater Program: Northern Gulf of Mexico Continental Slope Habitats and Benthic Ecology" (DGoMB). These cores were processed for radiochemical assay to determine particle reworking (bioturbation) and sedimentation rates in these sediments, pursuant to the research objective to investigate biological and physical processes that control the environmental setting for GOM benthic fauna. Ancillary objectives included the investigation of the role of macrofauna in both POC and fallout radionuclide inventories and organic carbon remineralization in the GOM. We have concluded the following based on the results of this work:

– $^{234}Th_{xs}$ penetration depths are between 0.5 and 4 cm, which coincides closely with the depth distribution of macrofauna and bioturbation coef-

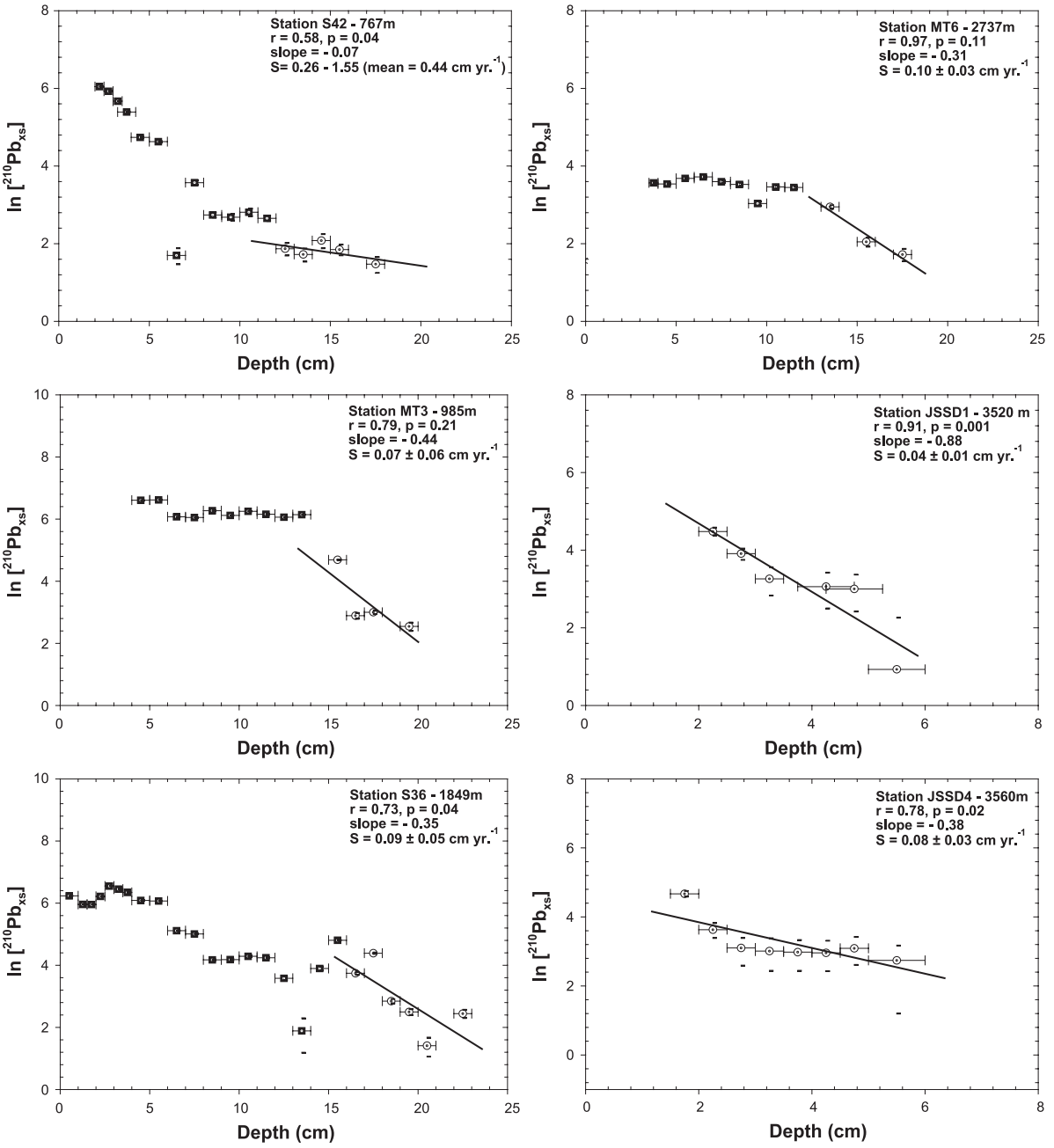

Fig. 3. $^{210}Pb_{xs}$ ([^{210}Pb (total)] – [^{210}Pb (supported) = ^{226}Ra]) profiles for all stations, all $^{210}Pb_{xs}$ data below the $^{234}Th_{xs}$ penetration depth is plotted. Sedimentation rates (S) were determined from the slope of $\ln[^{210}Pb_{xs}(z)] = \ln[^{210}Pb_{xs}(0)] - (\lambda/S)z$, using only those points below significant ^{239,240}Pu activity (open circles). Errors in ln $^{210}Pb_{xs}$ data are plotted for each point, but are often less than the size of the data symbol.

ficient values, D_b, range from approximately 2 to 30 cm^2/year.
- The ranges of apparent sedimentation and accumulation rates determined for these stations are 0.04–0.44 cm/year and 0.02–0.56 g/cm^2 year, respectively, showing that after approximately 1000 m water depth, these rates become essentially constant.
- POC inventories compared directly with macrofaunal densities illustrate the significant relationship ($r=0.96$, $p=0.003$) between organic carbon inventory and macrofaunal abundance.
- Macrofauna density significantly influences inventories of the fallout radionuclides $^{239,240}Pu$ and $^{210}Pb_{xs}$ ($r=0.91$, $p=0.01$; $r=0.80$, $p=0.05$, respectively), supporting our contention that high densities of macrofauna provide for a well mixed near surface sediment layer, wherein fallout radionuclides are more efficiently incorporated via mixing and adsorption into the sediment profile.

This research provides essential data on marine sedimentation within the slope and abyssal plain environments of the GOM, well outside the relatively well characterized Mississippi River Delta region. This work also provides additional insight into the coupled nature of organic carbon supply and benthic faunal abundances and in turn characterizes the importance of both of these variables with respect to the incorporation of fallout radionuclides into the marine sedimentary record. Future work focusing on these relationships elsewhere in the GOM and similar marine environments throughout the world is strongly encouraged.

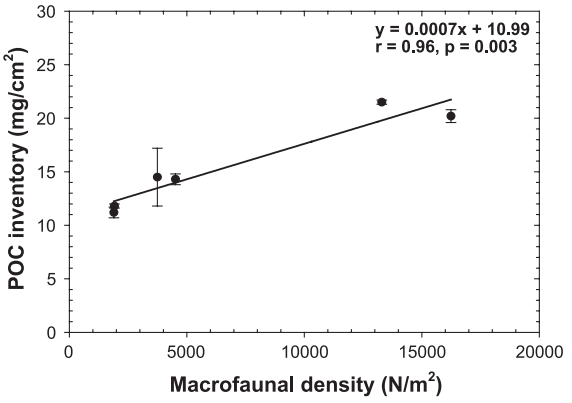

Fig. 4. Macrofauna densities versus POC inventories for each station, least squares fit applied; errors are plotted for POC inventory for each point, but are at times less than the size of the data symbol.

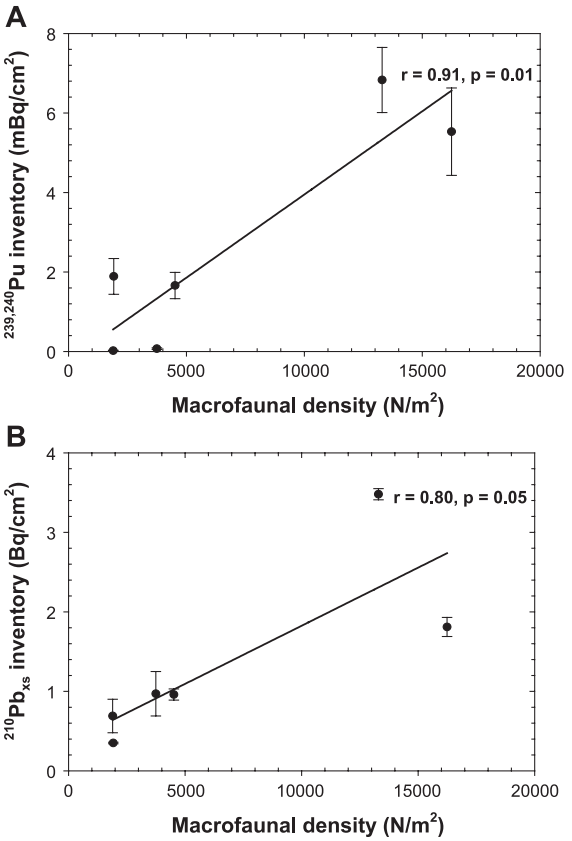

Fig. 5. (A, B) Macrofauna densities versus $^{239,240}Pu$ (A) and $^{210}Pb_{xs}$ (B) inventories for each station, least squares fit applied, errors are plotted for both radionuclide inventories for each point, but are at times less than the size of the data symbol.

Acknowledgements

Funding provided by the United States Mineral Management Service (Contract No. 1435-01-99-CT-30991) is gratefully acknowledged. Thanks are also extended to Ms. Kim Roberts, Ms. Kimberly Schindler and Ms. Michelle Spinelli for laboratory assistance, Mr. Gary Wolff for assistance with figures, the Texas Institute of Oceanography for its support, and to Drs. Mead Allison, Dave DeMaster and Reide Corbett who contributed to the improvement of this manuscript.

References

Anderson, R.F., Rowe, G.T., Kemp, P.F., Trumbore, S., Biscaye, P.E., 1994. Carbon budget for the mid-slope depocenter of the Middle Atlantic Bight. Deep-Sea Res. II 41 (2/3), 669–703.

Bacon, M.P., Cochran, J.K., Hirschberg, D., Hammar, T.R., Fleer, A.P., 1996. Export flux of carbon at the equator during the EqPac time-series cruise estimated from ^{234}Th measurements. Deep-Sea Res. II 43, 1133–1153.

Benoit, G., Patton, P.C., Arnold, C.L., 1999. Trace metals and radionuclides reveal sediment sources and accumulation rates in Jordan Cove. Connecticut. Estuaries 22 (1), 65–80.

Boland, G.S., Rowe, G.T., 1991. Deep-sea benthic sampling with the gomex box corer. Limnol. Oceanogr. 36 (5), 1015–1020.

Buesseler, K.O., Andrews, J.A., Hartman, M.C., Belastock, R., Chai, F., 1995. Regional estimates of the export flux of particulate organic carbon derived from thorium-234 during the JGOFS EQPAC program. Deep-Sea Res. II 41, 777–804.

DeMaster, D.J., Pope, R.H., Levin, L.A., Blair, N.E., 1994. Biological mixing intensity and rates of organic carbon accumulation in North Carolina Slope sediments. Deep-Sea Res. II 41, 735–753.

DeMaster, D.J., Thomas, C.J., Blair, N.E., Fornes, W.L., Plaia, G., Levin, L.A., 2002. Deposition of bomb ^{14}C in continental slope sediments of the Mid-Atlantic Bight: assessing organic matter sources and burial rates. Deep-Sea Res. II 49, 4667–4685.

Goodbred, S.L., Kuehl, S.A., 1998. Floodplain processes in the Bengal Basin and the storage of Ganges-Brahmaputra river sediment: an accretion study using ^{137}Cs and ^{210}Pb geochronology. Sediment. Geol. 121, 239–258.

Huntley, S.L., Wenning, R.J., Su, S.H., Bonnevie, N.L., Paustenbach, D.J., 1995. Geochronology and sedimentology of the Lower Passaic River, New Jersey. Estuaries 18 (2), 351–361.

Legeleux, F., Reyss, J.-L., Schmidt, S., 1994. Particle mixing rates in sediments of the northeast tropical Atlantic: evidence from $^{210}Pb_{xs}$, ^{137}Cs, $^{228}Th_{xs}$ and $^{234}Th_{xs}$ downcore distributions. Earth Planet. Sci. Lett. 128, 545–562.

Oktay, S.D., Santschi, P.H., Moran, J.E., Sharma, P., 2000. The 129-iodine bomb pulse recorded in Mississippi River Delta sediments: results from isotopes of I, Pu, Cs, Pb, and C. Geochim. Cosmochim. Acta 64 (6), 989–996.

Pope, R.H., Demaster, D.J., Smith, C.R., Seltmann Jr., H., 1996. Rapid bioturbation in equatorial Pacific sediments: evidence from excess ^{234}Th measurements. Deep-Sea Res. II 43, 1339–1364.

Radakovitch, O., Heussner, S., 1999. Fluxes and budget of ^{210}Pb on the continental margin of the Bay of Biscay (northeastern Atlantic). Deep-Sea Res. II 46, 2175–2203.

Ravichandran, M., Baskaran, M., Santschi, P.H., Bianchi, T.S., 1995a. History of trace metal pollution in Sabine-Neches Estuary, Texas. Environ. Sci. Technol. 29, 1495–1503.

Ravichandran, M., Baskaran, M., Santschi, P.H., Bianchi, T.S., 1995b. Geochronology of sediments of Sabine-Neches Estuary, Texas. Chem. Geol. 125, 291–306.

Rowe, G.T., Sibuet, M., Deming, J., Khripounoff, A., Tietjen, J., Macko, S., Theroux, R., 1991. Total sediment biomass and preliminary estimates of organic residence time in deep-sea benthos. Mar. Ecol., Prog. Ser. 79, 99–114.

Rutgers van der Loeff, M.M., Friedrich, J., Bathmann, V., 1997. Carbon export during the spring bloom at the Antarctic Polar Front, determined with the natural tracer ^{234}Th. Deep-Sea Res. II 44, 457–478.

Santschi, P.H., Li, Y.H., Bell, J., Trier, R.M., Kawtaluk, K., 1980. Plutonium in the coastal marine environment. Earth Planet. Sci. Lett. 51, 248–265.

Santschi, P.H., Allison, M., Asbill, S., Perlet, A.B., Cappellino, S., Dobbs, C., McShea, L., 1999. Sediment transport and Hg recovery in Lavaca Bay, as evaluated from radionuclide and Hg distributions. Environ. Sci. Technol. 33, 378–391.

Santschi, P.H., Presley, B.J., Wade, T.L., Garcia-Romero, B., Baskaran, M., 2001a. Historical contamination of PAH's, PCB's, DDT's, and heavy metals in Mississippi River Delta, Galveston Bay and Tampa Bay sediment cores. Mar. Environ. Res. 52, 51–79.

Santschi, P.H., Guo, L., Asbill, S., Allison, M., Kepple, A.B., Wen, L.S., 2001b. Accumulation rates and sources of sediments and organic carbon on the Palos Verdes shelf based on radioisotopic tracers (^{137}Cs, ^{239,240}Pu, ^{210}Pb, ^{234}Th, ^{238}U and ^{14}C). Mar. Chem. 73, 125–152.

Somayajulu, B.L.K., Rhushan, R., Sarkar, A., Burr, G.S., Jull, A.J.T., 1999. Sediment deposition rates on the continental margins of the eastern Arabian Sea using ^{210}Pb, ^{137}Cs and ^{14}C. Sci. Total Environ. 237/238, 429–439.

Stull, J.K., Swift, D.J.P., Niedoroda, A.W., 1996. Contaminant dispersal on the Palos Verdes continental margin: I. Sediment and biota near a major California wastewater discharge. Sci. Total Environ. 179, 73–90.

Yeager, K.M., Santschi, P.H., 2003. Invariance of isotope ratios of lithogenic radionuclides: more evidence for their use as sediment source tracers. J. Environ. Radioac. 69, 159–176.

Zuo, Z., Eisma, D., Gieles, R., Beks, J., 1997. Accumulation rates and sediment deposition in the northwestern Mediterranean. Deep-Sea Res. II 44 (3–4), 560–597.